Laser ultrasonics in a multilayer structure: Plane wave synthesis and inverse problem for nondestructive evaluation of adhesive bondings

R. Hodé, S. Raetz, N. Chigarev, J. Blondeau, N. Cuvillier, V. Gusev, M. Ducousso, V. Tournat, et al.

Citation: The Journal of the Acoustical Society of America **150**, 2076 (2021); doi: 10.1121/10.0005975
View online: https://doi.org/10.1121/10.0005975
View Table of Contents: https://asa.scitation.org/toc/jas/150/3
Published by the Acoustical Society of America

JASA ARTICLE

Laser ultrasonics in a multilayer structure: Plane wave synthesis and inverse problem for nondestructive evaluation of adhesive bondings

R. Hodé,[1,a),b)] S. Raetz,[1,c)] N. Chigarev,[1,d)] J. Blondeau,[1] N. Cuvillier,[2,e)] V. Gusev,[1,f)] M. Ducousso,[2,g)] and V. Tournat[1,h)]

[1]*Laboratoire d'Acoustique de l'Université du Mans, Unité Mixte de Recherche 6613, Institut d'Acoustique–Graduate School, CNRS, Le Mans Université, Le Mans, France*

[2]*Safran Tech, Rue des Jeunes Bois–Châteaufort, 78772 Magny-les-Hameaux, France*

ABSTRACT:

A laser ultrasonic method is proposed for the nondestructive evaluation of bonded assemblies based on the analysis of elastic plane waves reflected from the bonding interface. Plane waves are numerically synthesized from experimentally detected cylindrical waves. Several angles of incidence with respect to the bonding interface are achieved by varying the delay in the synthesis step. An inverse problem using these plane waves is then solved to identify the normal and transverse interfacial stiffnesses that model the mechanical coupling between two bonded media. The semi-analytic model developed and detailed in Hodé *et al.* [J. Acoust. Soc. Am. 150, 2065 (2021)] is used to create the database that contains simulated laser-generated ultrasounds required to solve the inverse problem. The developed method is first validated with semi-analytic simulated input data where Gaussian noise has been added. Next, the method is applied using signals acquired on an aluminum alloy plate and on assemblies (with and without adhesion defects) made of two aluminum alloy plates bonded by an aeronautical structural epoxy adhesive film. Differences between the identified values of interfacial stiffnesses distinguish the three samples and obtain quantitative values to characterize the adhesive bonding. © *2021 Acoustical Society of America.*

https://doi.org/10.1121/10.0005975

(Received 11 December 2020; revised 25 July 2021; accepted 5 August 2021; published online 22 September 2021)

[Editor: Michael R. Haberman] Pages: 2076–2087

I. INTRODUCTION

In aeronautics, lighter aircraft structures are essential to reduce fuel consumption and emissions. Structural adhesive bonding is one of the solutions to meet this need. Indeed, it has numerous advantages over conventional assembly techniques, such as riveting and welding. A better stress distribution can be achieved between the assembled parts. Furthermore, it is the best method for joining composite materials with a high strength-to-weight ratio. However, one of the technological limitations currently reducing the significant deployment of this technique is the lack of nondestructive evaluation (NDE) methods[1–3] to certify the mechanical strength of the bonding.

In the past 50 years, a large number of nondestructive methods have been investigated in the literature. Among the various studied approaches, such as infrared thermography[4,5] and quantitative techniques based on laser-generated shock waves,[6,7] ultrasonic methods are of great interest, as elastic waves interact mechanically with the bonding without damaging it. These methods can be divided in two main categories according to whether they are based on bulk or guided waves. Concerning the studies dealing with bulk waves, experiments have used the reflection of ultrasound at normal and oblique incidence with respect to the adhesive joint.[8–11] Transmission measurements have also been achieved experimentally with immersed[12] and air-coupled ultrasonic transducers.[13] Theoretical studies have been carried out to model bonded elastic media to investigate the effects of bonding defects on reflection and transmission coefficients.[14–17] Lavrentyev and Rokhlin,[18] Wang *et al.*,[19] and then Baltazar *et al.*[20] successively developed an inversion method to identify parameters related to the bonding properties from the reflection spectra acquired at two angles of incidence (normal and oblique). With regard to ultrasonic methods based on guided waves, theoretical and experimental studies have used shear horizontal modes[21,22] and Lamb modes.[23,24] These methods allowed an averaged evaluation of the bonding quality along the propagation path of the guided waves. For a better localization of bonding defects, all-optical methods that are based on laser-generated zero group velocity (ZGV) Lamb modes,[25] which are sharp local resonances at well-defined frequencies, have been experimentally investigated.[26–28] These laser ultrasonic techniques

[a)]Electronic mail: romainod@gmail.com, ORCID: 0000-0001-7883-9621.
[b)]Also at: Safran Tech, Rue des Jeunes Bois–Châteaufort, 78772 Magny-les-Hameaux, France.
[c)]ORCID: 0000-0003-3683-8764.
[d)]ORCID: 0000-0002-2902-9363.
[e)]ORCID: 0000-0002-1577-3458.
[f)]ORCID: 0000-0002-2394-7892.
[g)]ORCID: 0000-0002-4014-6747.
[h)]ORCID: 0000-0003-4497-5742.

https://doi.org/10.1121/10.0005975

are of real interest for industrial applications because of the fully contactless nature of the measurements.

In this paper, a laser ultrasonic method is presented for the quantitative NDE of adhesive bonding. The work is based on the synthesis of elastic plane waves developed by Reverdy and Audoin.[29,30] This postprocessing method has originally been designed to find the elastic coefficients of isotropic or anisotropic plates using laser-generated ultrasound. The times-of-flight (TOFs) of the synthesized plane waves were used to solve an inverse problem on the basis of the Christoffel equation. Here, this method is applied to identify the mechanical coupling conditions between two bonded elastic media with known elastic coefficients. Not only the TOFs but also the amplitudes of the synthesized reflected plane waves are gathered for different angles of incidence with respect to the bonding interface. Moreover, not only the first reflection at the bonding interface is considered but also the multiple reflections of elastic waves that occur as time goes on. Mode conversions due to the reflection of elastic waves at the bonding interface are therefore accounted for. An inverse problem is then solved to identify the normal and transverse interfacial stiffnesses used to model the bonding. These interfacial stiffnesses are homogeneous surface densities of spring stiffnesses expressed in $\mathrm{kN\,mm^{-3}}$, i.e., the bonded interfaces are assumed to have homogeneous properties. One of the novelties of the developed approach concerns the creation of the database to solve the inverse problem. A semi-analytic model that we developed and have detailed in Ref. 49 is used to simulate the propagation of laser-generated ultrasounds in bonded assemblies. A large number of semi-analytic simulations were conducted to generate a database that contains simulated signals for different values of interfacial stiffnesses used to model bonding. The current work aims to present a specific application of our semi-analytic model for the NDE of bondings. This approach, which combines laser ultrasonic experiments and the synthesis of elastic plane waves as a postprocessing technique, is tested on experimental signals measured on bonded assemblies made from materials encountered in aeronautics.

The outline of this paper is as follows. In Sec. II, the postprocessing method to synthesize plane waves is described, and the application of this technique for the NDE of adhesive bonding is presented. In Sec. III, two methods are introduced to simulate the temporal evolution of the amplitudes of the synthesized plane waves reflected from the here-investigated interface between two bonded media. The choice of a semi-analytic approach to solve the direct problem is justified, and numerical results are provided. In Sec. IV, the algorithm used to solve the inverse problem to identify the values of normal and transverse interfacial stiffnesses, which model the mechanical coupling between two bonded media, is detailed. The identification process is first validated using simulated data to which noise has been added. Next, in Sec. V the inverse problem is solved using experimental data acquired for a free-standing aluminum alloy plate and for two bonded assemblies (Al/epoxy/Al) with and without adhesion defects. The epoxy layer was, in both cases, an industrial aeronautical adhesive. Both assemblies, similar in geometry and constituents yet different in adhesion level were undistinguishable when evaluated with conventional ultrasonic inspection techniques. The identification of the interfacial stiffnesses with the proposed method is presented. Its ability to nondestructively characterize adhesive bondings and, therefore, to distinguish different adhesion levels is demonstrated.

II. PLANE WAVE SYNTHESIS FOR THE NDE OF ADHESIVE BONDINGS

One advantage of laser ultrasound generation in the thermoelastic regime is that the surface of the inspected material is not locally degraded, in contrast to the ablation regime. However, the elastic waves generated in this regime are of relatively low amplitudes, which can make optical signal detection difficult and result in a relatively poor signal-to-noise ratio (SNR). For these reasons, different techniques have been developed to increase the amplitude of laser-generated ultrasound and to improve the directivity pattern of optoacoustic sources. Plane wave generation is one of the methods to address this issue.

For absorbing materials, the easiest way to experimentally and nondestructively generate plane waves in laser ultrasonics is to use a thermoelastic source with lateral dimensions that are very large compared to the achievable wavelength. The drawback of that approach is that only plane waves propagating in a direction normal to the generation surface are made possible. Two main experimental techniques that steer the propagation direction of plane waves along any angle have been reported in literature. One approach is based on a moving laser source that continuously sweeps the surface of a medium at subsonic, transonic, or supersonic velocities. Berthelot and Busch-Vishniac[31] applied this technique for the experimental generation of plane waves in a freshwater tank. The mobile thermoacoustic source on the water surface was created by the reflection of a laser beam from a rotating mirror. Ing *et al.*[32] used an acousto-optic cell working under the Bragg mode to generate a moving laser source at the surface of an aluminum half cylinder. Another approach to launch plane waves is based on a set of photoacoustic sources separated in space and time. These laser ultrasonic methods are close to those developed in conventional ultrasound with the use of phased array transducers.[33] Steckenrider *et al.*[34] used the propagation of a single laser pulse in an optical delay system consisting of a White cell cavity[35] and a graded beamsplitter to generate up to ten spatially and temporally separated laser sources. Another technique that requires only one laser beam was based on the redirection of a laser pulse into several optical fibers of different lengths, resulting in phase shifts.[36–38] Furthermore, multiple laser beams were used to design a phased array of laser sources. Noroy *et al.* carried out experiments with a multiple-beam Q-switched neodymium-doped yttrium aluminum garnet (Nd:YAG) laser capable of delivering 16 optical pulses.

Laser-generated ultrasonic phased arrays were performed by the authors in the ablation regime[39] and in the thermoelastic regime.[40,41] Murray *et al.*[42] followed a similar approach with ten Nd:YAG lasers cavities.

Although laser-generated plane waves are experimentally achievable, these techniques are difficult to realize in practice and require the use of more complicated systems than those with two laser beams, i.e., one for ultrasound generation and one for detection. Therefore, an alternative approach that is based on the synthesis of plane waves in a postprocessing step has been chosen and is detailed as follows.

A. Description of the plane wave synthesis

To synthesize plane waves from divergent laser-generated ultrasound, a method has been developed by Reverdy and Audoin.[29,30] They have used it to measure the elastic coefficients of anisotropic materials by solving an inverse problem based on the Christoffel equation. The first step of this technique is the acquisition of temporal signals. A laser line source of infinite length in the $\mathbf{x}_3$ direction is moved over the sample surface in $2N+1$ positions with a constant δx-step. At each $i \in [-N, N]$ position, laser-generated ultrasound is emitted in the sample, and the normal displacement of the surface is measured at the $i=0$ position. Therefore, for each generation location, a temporal signal $s_i(t)$ is recorded. The second step deals with the postprocessing of the acquired data to synthesize plane waves. A constant time delay δt is imposed between the signals $s_i(t)$ and $s_{i+1}(t)$. Then, a sum of all the signals is achieved to obtain

$$s(t) = \sum_{i=-N}^{N} s_i(t + i\delta t), \tag{1}$$

where $s(t)$ corresponds to the signal that would have been experimentally recorded at the $i=0$ position if a phased array of laser sources had generated plane waves in the linear domain, i.e., when the superposition principle is valid. The time delay δt directly selects the propagation angle φ_n of the synthesized plane wave of n-polarization, given by

$$\sin(\varphi_n) = \frac{k_s}{k_n}, \quad n = \{\mathrm{L}, \mathrm{T}\}, \tag{2}$$

with L and T denoting the longitudinal and transverse polarizations of the elastic waves, respectively, for an isotropic material. The wavenumber $k_s = \omega\,\delta t/\delta x$ is defined by ω as the angular frequency; δx as the fixed spatial step; and δt as the time delay, which is an adjustable parameter. The wavenumber of the synthesized plane wave is $k_n = \omega/c_n$, with c_n being the phase velocity of the wave having an n-polarization. Note that the synthesized wavefield is referred to as the synthesized plane wave to focus on the role of the main lobe of the synthesized wavefield that can be seen as a plane wave propagating at an angle φ_n, which is named propagation angle in the following. Interestingly, this selection rule of two propagation angles for longitudinal and transverse waves can also be seen in another way. Since the sample considered here is multilayered, it is a waveguide along the $\mathbf{x}_2$ direction. Imposing the time delay δt is therefore equivalent to select guided waves propagating along the $\mathbf{x}_2$ direction, with a wavevector component along that direction of $k_s = \omega\,\delta t/\delta x$. Next, the TOFs and amplitudes of the synthesized plane waves are obtained by convolving the signal $s(t)$ with a complex Morlet wavelet.[29] To identify the elastic coefficients of an anisotropic plate, the TOF of the synthesized plane waves was measured either in transmission[29] or in reflection.[30]

B. Application for the NDE of adhesive bondings

In this paper, the aim is to quantify the mechanical strength of structural adhesive bonding using this approach. Thus, not only the arrival times but also the amplitudes of the plane waves reflected from the bonding interface are considered. The studied structure is represented in Fig. 1(a) and is composed of an elastic plate of thickness h_1 bonded on a thicker medium of thickness h_2. Both media are assumed to be linear, homogeneous, and isotropic. In addition, h_2 is assumed to be much larger than h_1; hence, the lower elastic medium is modeled acoustically as a half-space, i.e., the following treatment is applied over a measurement time, ensuring that no wave reflected from the bottom surface of the lower medium is in the signal. Furthermore, the acoustic wavelengths that are considered later are assumed to be greater than the thickness of the adhesive joint. Thus, normal (K_N) and transverse (K_T) distributions of interfacial stiffnesses, illustrated by springs in Fig. 1(a), are used to model the bonding.[16,43,44] This modeling is deduced from the simplification of the transfer matrix formalism.[45–48] It allows the coupling of displacements and stresses between media I and II.

The sum of all the signals $s_i(t + i\delta t)$ in Eq. (1) is illustrated in Fig. 1(b). The application of time delay δt in a postprocessing step leads to constructive and destructive interferences that result in the synthesis of plane waves. As shown in the slowness diagram in Fig. 1(c), the choice of the wavenumber k_s in Eq. (2), linked to the ratio $\delta t/\delta x$, favors the generation of a longitudinal plane wave L and a transverse one T of defined propagation angles φ_n. Therefore, the synthesized plane waves that propagate in medium I are represented in Fig. 1(a). Two incident plane waves L and T are reflected from the interface according to Snell's laws. Thus, the longitudinal plane wave L is reflected as a wave that retains the same polarization [which is noted 2L in Fig. 1(a)] and a wave with a polarization conversion (LT). It is the same for the incident transverse plane wave T, which is reflected as transverse (2T) and longitudinal (TL) plane waves. Then, these four waves are reflected from the free surface of medium I, in $x_1 = 0$, and so on.

The interest of using this technique is that the amplitudes of the reflected waves are related to the reflection coefficients from the bonding interface. In fact, the expressions of these coefficients are defined not only by the

https://doi.org/10.1121/10.0005975

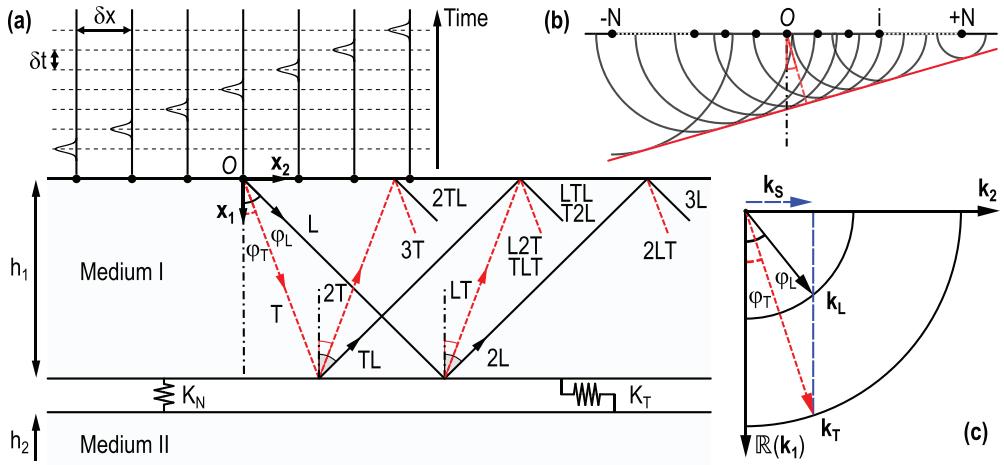

FIG. 1. (Color online) (a) Representation of the elastic plane waves that are synthesized in medium I. First, a laser line source of infinite length in the $\mathbf{x}_3$ direction is moved over the sample surface in $2N+1$ positions with a constant δx step. Second, a time delay δt is applied between the laser pulses in postprocessing to synthesized longitudinal (L) and transverse (T) plane waves. (b) The application of delays between the $2N+1$ sources leads to constructive and destructive interferences between the divergent elastic waves, resulting in the generation of a plane wave. (c) Slowness diagram of the L and T plane waves that are synthesized by imposing the wave vector $k_s = \omega\,\delta t/\delta x$, with ω as the angular frequency.

mechanical properties of media I and II but also by the coupling conditions at the interface. Thus, a modification of the mechanical coupling between two media leads to an evolution of the reflection coefficients and, consequently, to a change in the amplitudes of the reflected plane waves.

The strategy adopted in this paper is to solve an inverse problem to find the normal (K_N) and transverse (K_T) interfacial stiffnesses with the amplitudes of the reflected plane waves. This requires the calculation of the direct problem, i.e., finding the normal displacement of the surface as a function of time, knowing the interfacial stiffnesses. This will be detailed in Sec. III.

III. SOLVING THE DIRECT PROBLEM

Two approaches were studied to solve the direct problem: one based on analytic formulas taking the directivity pattern of an array of thermoelastic sources into account and another based on semi-analytic simulations to numerically solve the electromagnetic, thermal, and elastodynamic problems. These two methods are presented in Secs. III A and III B, respectively. In addition, the choice of the second method rather than the first for the subsequent resolution of the inverse problem will be justified.

A. Analytic formulation

The first approach used to solve the direct problem was to calculate the amplitudes of the reflected plane waves using analytic formulas, as reported in literature.[41,49,50] The goal was to find the theoretical amplitudes, as a function of the propagation angle φ_n defined in Eq. (2), of all plane waves reflected from the bonding interface illustrated in Fig. 1(a): 2L, LT, TL, 2T, etc. Assuming that both the bonding interface and the observation point are in the far field, the amplitudes of these reflected plane waves can be obtained by considering the directivity pattern of the array of thermoelastic sources, the propagation path of plane waves, the reflections from the bonding interface, and the laser detection at the free surface of medium I. However, in the cases we are studying, the observation point is in the near field of the thermoelastic sources because the thickness of medium I is of the order of a millimeter. It implies that the directivity pattern of the thermoelastic sources, notably calculated in the far field by Raetz *et al.*,[51] cannot be used here. In addition, this analytic approach leads to complicated formulas where a multitude of plane wave reflections have to be accounted for. Indeed, as shown in Fig. 1(a), an incident plane wave is reflected as two plane waves of different polarization at each reflection from the bonding interface or the upper free surface of medium I. Hence, the number of analytic formulas to calculate all the reflected plane waves increases rapidly with time.

For all these reasons, another approach has been selected to solve the direct problem. The choice was made to use semi-analytic simulations to numerically solve the electromagnetic, thermal, and elastodynamic problems. This method, presented in Sec. III B and fully described in Ref. 49 (semi-analytic model and simulated examples), provides fast and accurate simulated data. Moreover, it allows solving the multiphysics problem without using the far-field assumption, unlike the previous approach that was based on directivity patterns of optoacoustic sources.

B. Semi-analytic model

The resolution of the direct problem, i.e., the simulation of laser-generated ultrasound in the bonded structure, was achieved with a semi-analytic method. This numerical approach was notably inspired by the work of Audoin and Guilbaud[52] and Audoin *et al.*[53] This method was used to simulate acoustic waves generated by a laser line source based on Fourier transform. In Ref. 48, this model was extended to the simulation of laser-generated elastic waves in a multilayer structure, where the electromagnetic,

thermal, and elastodynamic problems were numerically solved. It allows the displacement field in the upper and lower media of the multilayer structure to be obtained. The method provides accurate results in a relatively short computing time compared with other numerical techniques, such as the finite element method (FEM)[54,55] or the finite difference method (FDM).[56] Accuracy and rapidity are two advantages of real interest for inverse problem solving and justify this choice for the cases studied in this paper. Obviously, if more complex geometries than layered plates with parallel surfaces have to be investigated, the FEM or FDM are preferred.

Concerning the possibilities offered by the semi-analytic model detailed in Ref. 48, a tilted laser line source of infinite length in the $\mathbf{x}_3$ axis can be considered. The temporal and spatial Gaussian profiles of this thermoelastic source are taken into account. The electromagnetic transmission and reflection of the incident laser beam in the multilayer are calculated, and the optical penetration is accounted for. The solution to the electromagnetic problem allows the power densities dissipated into heat, which are used as source terms for solving the heat diffusion problem, to be obtained. Conduction and convection phenomena are considered to find the amplitudes of the thermal waves that are diffusing in the structure. Next, analytic solutions of the displacement fields generated by the thermal expansion are determined in the Fourier domain. Subsequently, a double numerical inverse Fourier transform in space and time is performed to find the displacement field in the time domain. The thermal coupling between media I and II is obtained with a thermal resistance, which is defined from the thermal properties of all the sublayers inserted between media I and II. Electromagnetic and mechanical coupling conditions are taken into account with transfer matrices.[45,46]

In Secs. IV and V, this numerical model is applied to solve inverse problems involving bonded aluminum substrates. Thus, further assumptions are formulated for the resolution of electromagnetic, thermal, and elastodynamic problems.

First, perfect electromagnetic and thermal coupling between media I and II is assumed. Indeed, the thermoelastic source remains localized at the surface of medium I because (i) the optical penetration depth of a normal incident laser beam in aluminum is about 4.7 nm along the $\mathbf{x}_1$ axis (@ $\lambda_{\text{opt}} = 532$ nm) and (ii) the thermal penetration depth is equal to $\sqrt{2D_{11}/\omega} = 2.0$ μm with the thermal diffusivity of aluminum $D_{11} = 62$ μm^2 μs^{-1} and the angular frequency $\omega = 2\pi f$ rad μs^{-1}, with $f = 5$ MHz.[48] Both optical and thermal penetration depths are negligible compared with the thickness of medium I, which is of the order of a millimeter. Thus, perfect conditions of electromagnetic and thermal coupling can be imposed between media I and II because none of these waves are interacting with the bonding interface.

Second, the mechanical coupling between two aluminum substrates is modeled with normal (K_N) and transverse (K_T) interfacial stiffnesses[43] [shown in Fig. 1(a)]. This model results from the simplification of the transfer matrix[45,46,48] that links displacements and stresses between the upper and lower surfaces of an elastic plate.[57] Assuming that the acoustic wavelengths are large with respect to the adhesive joint thickness, this transfer matrix can be simplified into an identity matrix having two extradiagonal terms: K_N and K_T. It implies continuity of stresses (σ_{11}, σ_{12}) and discontinuity of displacements (u_1, u_2) at the interface between media I and II at $x_1 = h_1$ [see Fig. 1(a)], which gives

$$\sigma_{11}^{\text{I}}|_{x_1=h_1} = \sigma_{11}^{\text{II}}|_{x_1=h_1} = K_N(u_1^{\text{II}}|_{h_1} - u_1^{\text{I}}|_{h_1}), \tag{3}$$

$$\sigma_{12}^{\text{I}}|_{x_1=h_1} = \sigma_{12}^{\text{II}}|_{x_1=h_1} = K_T(u_2^{\text{II}}|_{h_1} - u_2^{\text{I}}|_{h_1}). \tag{4}$$

C. Results of semi-analytic simulations

Numerical results achieved with this semi-analytic model are plotted in Fig. 2. Note that the horizontal dashed gray line stands for the interface between media I and II. The bilayer structure is composed of an aluminum plate of thickness mm mechanically coupled to a semi-infinite aluminum medium. Both media are considered homogeneous, linear, and isotropic of density $\rho = 2.7\,10^3$ kg m^{-3} and elastic coefficients of $C_{11} = 109.9$ GPa and $C_{66} = 26.5$ GPa. Concerning the thermoelastic source, a normal incident laser line pulse of infinite length along the $\mathbf{x}_3$ axis is considered. The pulse duration is $\tau_p = 8$ ns, which corresponds to the full width at half maximum (FWHM) of the temporal Gaussian profile. The width of the laser line source along the $\mathbf{x}_2$ axis is $a_s = 0.2$ mm, which corresponds to the FWHM of the spatial Gaussian profile. Three cases are simulated for different values of normal and transverse interfacial stiffnesses. The first case is the simulation of the

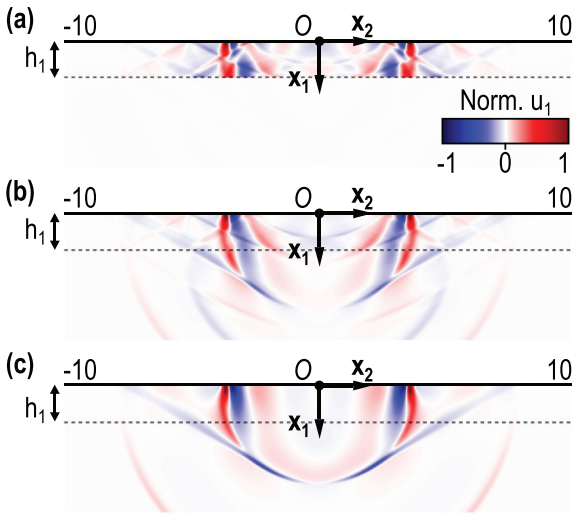

FIG. 2. (Color online) Results of semi-analytic simulations (Ref. 57) in three different cases. Snapshots at $t = 1.25$ μs of the normalized (Norm.) normal displacement u_1 in a bilayer structure with normal and transverse interfacial stiffnesses [illustrated in Fig. 1(a)] of (a) $K_N = K_T = 10^{-3}$ kN mm^{-3} for the decoupling case, (b) and $K_T = 10^1$ kN mm^{-3} for the intermediate coupling, and (c) $K_N = K_T = 10^5$ kN mm^{-3} for the high mechanical coupling between media I and II.

https://doi.org/10.1121/10.0005975

normalized normal displacement $u_1(x_1, x_2, t)$ with $K_N = K_T = 10^{-3}\,\mathrm{kN\,mm^{-3}}$. This is equivalent to a mechanical decoupling between media I and II, i.e., ultrasonic waves are fully reflected from the interface, as shown in Fig. 2(a). The second case deals with an intermediate mechanical coupling with $K_N = 10^{3}\,\mathrm{kN\,mm^{-3}}$ and $K_T = 10^{1}\,\mathrm{kN\,mm^{-3}}$. In Fig. 2(b), simulated elastic waves are reflected from the interface at $x_1 = h_1$ and are transmitted into medium II. The third case is the simulation of ultrasonic propagation when $K_N = K_T = 10^{5}\,\mathrm{kN\,mm^{-3}}$, which corresponds to a high mechanical coupling. Since the two media are the same, a total transmission of the elastic waves at the interface is observed in Fig. 2(c). This simulation is analogous to what would have been obtained in an elastic half-space.

Such numerical results obtained with the semi-analytic model are the basis of the here-proposed method to solve the inverse problem to obtain a quantitative estimate of the adhesive bonding through values of K_N and K_T.

IV. RESOLUTION OF INVERSE PROBLEMS WITH SIMULATED DATA

An inverse method is proposed to identify the values of interfacial stiffnesses K_N and K_T using the amplitudes of the synthesized plane waves reflected from the bonding interface. The method is illustrated in Fig. 3 and is based on the two previous sections: the plane wave synthesis in Sec. II and the resolution of the direct problem in Sec. III. First of all, the plane wave synthesis is applied on a B-scan, which represents the normal displacement of the surface as a function of time t and position x_2. A large number of delays δt are imposed on these temporal signals to synthesize plane waves with different propagation angles φ_n with $n = \{\mathrm{L}, \mathrm{T}\}$. The adjustable parameter to control this angle is defined as $1/V_S = \delta t/\delta x$ in Fig. 3, with δx the fixed spatial step of the B-scan along the $\mathbf{x}_2$ axis and δt the delay that can be modified. These input data, which depend on time t and the adjustable parameter $1/V_S$ (see Fig. 3), are then compared to a database of a set of semi-analytic simulations with different values of interfacial stiffnesses K_N and K_T. Thus, the normal and transverse interfacial stiffnesses are identified by finding the minimum of a cost function, which will be defined in the following.

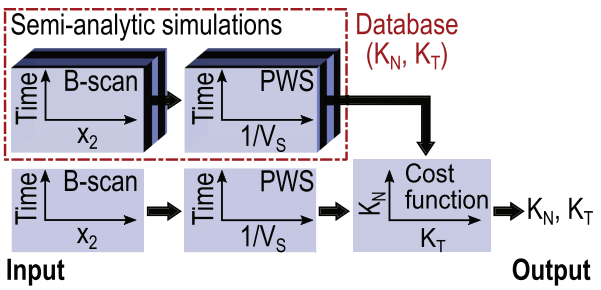

FIG. 3. (Color online) Diagram of the method to solve the inverse problem. The input data are B-scans where the plane wave synthesis (PWS) is applied. They are then compared to a database of semi-analytic simulations for different values of interfacial stiffnesses. The minimum of the cost function is finally searched to identify the values of K_N and K_T, which gives the lowest MSE between the input and the database.

The algorithm presented in Fig. 3 was tested with simulated input data before being used with experimental input data in Sec. V. This ensures that the inverse method works with input signals that have known interfacial stiffnesses. Furthermore, these simulated temporal signals were noised to get closer to experimentally measured waveforms. Three cases have been studied with different values of normal and transverse interfacial stiffnesses to represent three main situations: low, intermediate, and high mechanical coupling between media I and II. The first case dealt with low values of interfacial stiffnesses $K_N = K_T = 10^{-3}$ kN mm^{-3}. In this specific situation, the mechanical coupling was so weak that the elastic waves were fully reflected from the interface and no waves were transmitted in medium II [see simulation results in Fig. 2(a)]. Hence, this simulation was similar to that obtained for laser-generated ultrasound in an aluminum plate. Concerning the input data of the algorithm, a B-scan was simulated, with the semi-analytic model[48] succinctly presented in Sec. III B. Gaussian noise was applied to the temporal signals to be closer to an experimental case with a SNR ≈ 20 dB. Next, the plane wave synthesis was applied on these temporal signals following the sum introduced in Eq. (1). The delay δt between the signals $s_i(t)$ and $s_{i+1}(t)$ was applied in the Fourier domain by multiplying the fast Fourier transform of $s_i(t)$ by $e^{\jmath\omega i\delta t}$, with $\jmath$ the imaginary number, ω the angular frequency, and $i \in [-N, N]$ the source position shown in Fig. 1(b). For each propagation angle imposed by the delay δt, the summed signal $s(t)$ was convolved, with a complex Morlet wavelet having a center frequency of 5 MHz and a bandwidth at -3 dB equal to 4 MHz. This allows detection of the TOF and the amplitudes of the synthesized plane waves reflected from the interface. As the laser pulse generates wideband ultrasonic waves, the convolution by the complex Morlet wavelet acts as a bandpass filter to avoid considering high-frequency waves whose wavelengths are too short to be accurate for the model of the bonded assembly with interfacial stiffnesses. By varying the parameter $1/V_S = \delta t/\delta x$ between $\pm 0.2\,\mu$s mm^{-1} with a $3.2 \times 10^{-3}\,\mu$s mm^{-1} step, 129 propagation angles were imposed. This allowed the synthesis of longitudinal plane waves with propagation angles φ_L up to $\pm 90°$ and transverse plane waves with φ_T between $\pm 40°$. Indeed, beyond this angle, transverse waves of relatively low amplitudes were generated according to the directivity pattern of a thermoelastic source.[58] These postprocessed signals were then compared to a database of 1089 semi-analytic simulations with different values of K_N and K_T from 10^{-3} to 10^{5} kN mm^{-3}, with a step of $10^{0.25}$ kN mm^{-3}. It took about 30 h to compute this complete database on a laptop (Intel® Core™ i7-6500U central processing unit at 2.5 GHz, 16 GB random access memory; Intel Corporation, Santa Clara, CA). Comparisons were made using a cost function based on the mean squared error (MSE) between the results of the plane wave synthesis applied on the input data and the simulations of the database.

For the first studied case, where the input values were $K_N = K_T = 10^{-3}$ kN mm^{-3} [simulation in Fig. 2(a)], the cost function is provided in Fig. 4(a). The identified values of K_N and K_T were found when this function was minimum. This is represented by the red rectangle in Fig. 4(a), considering an uncertainty margin of ±0.1 dB on the minimum value of the cost function. This margin was chosen to account for uncertainties due to the addition of noise to the input data, which results in very small local variations of the cost function compared with those observed on a more global scale. This uncertainty margin of ±0.1 dB is equal to the standard deviation obtained after 100 successive resolutions of the inverse problem with randomly generated Gaussian noise added on the simulated B-scans and used as input data. The identified values of K_N and K_T are reported in Table I. In this case, the cost function is effectively the lowest for low values of interfacial stiffnesses in the range $[10^{-3}, 10^{-0.5}]$ kN mm^{-3} for K_N and $[10^{-3}, 10^{-0.75}]$ kN mm^{-3} for K_T. The fact that the identified values are within a given range is due not only to the added noise, as already discussed, but also to the fact that the reflection coefficients

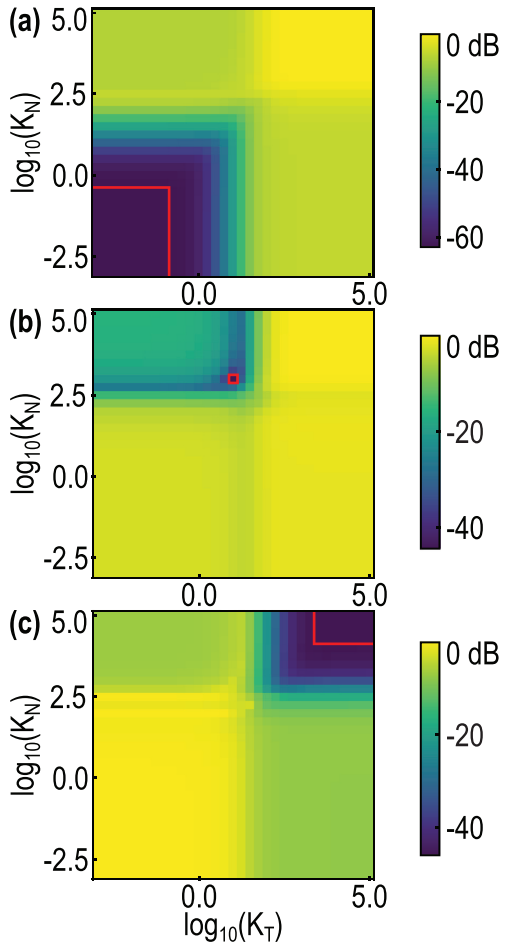

FIG. 4. (Color online) Cost functions (in dB) obtained when the plane wave synthesis is applied on simulated B-scans, with the addition of noise, for interfacial stiffnesses of (a) $K_N = K_T = 10^{-3}$ kN mm^{-3}, (b) $K_N = 10^3$ kN mm^{-3} and $K_T = 10^1$ kN mm^{-3}, Ballard (c) $K_N = K_T = 10^5$ kN mm^{-3}. The red rectangles indicate the location of the minimum of each cost function with an uncertainty margin of ±0.1 dB.

TABLE I. Results obtained by solving the inverse problem with noisy simulations as input data.[a]

	Input data		Identified parameters	
Simulation data	K_N	K_T	K_N	K_T
Low coupling	10^{-3}	10^{-3}	$[10^{-3}, 10^{-0.5}]$	$[10^{-3}, 10^{-0.75}]$
Intermediate coupling	10^3	10^1	10^3	10^1
High coupling	10^5	10^5	$[10^{4.25}, 10^5]$	$[10^{3.75}, 10^5]$

[a]Three different cases were processed for input values of K_N and K_T given in kN mm^{-3}: low, intermediate, and high mechanical coupling between media I and II. The interfacial stiffnesses identified using the minima of the cost functions are reported.

of the interface are not sensitive enough to small variations in mechanical coupling when interfacial stiffnesses are already low (i.e., <1 kN mm^{-3}). For the intermediate mechanical coupling case, where the cost function is plotted in Fig. 4(b), it is different. The minimum of the cost function is exactly equal to the value of the input interfacial stiffnesses, which are $K_N = 10^3$ kN mm^{-3} and $K_T = 10^1$ kN mm^{-3}. Thus, the reflection coefficients are highly sensitive to a change of mechanical coupling in this range of interfacial stiffnesses. For the high mechanical coupling case, the cost function is represented in Fig. 4(c). The identified values of interfacial stiffnesses are in the range $[10^{4.25}, 10^5]$ kN mm^{-3} for K_N and $[10^{3.75}, 10^5]$ kN mm^{-3} for K_T. This is consistent with the input values of interfacial stiffnesses that were $K_N = K_T = 10^5$ kN mm^{-3}. As in the case of low mechanical coupling, the reflection coefficients are less sensitive to small variations of mechanical coupling when interfacial stiffnesses are already high (i.e., >1 MN mm^{-3}); that is why the identified values are given within a particular range in Table I.

The interest of using the plane wave synthesis to compare the input data to the database and not to directly compare the B-scans (as it could be thought by looking at Fig. 3) is justified for two main reasons. First, the application of the plane wave synthesis implies a sum on all temporal signals [see Eq. (1)] of the B-scan between ±16 mm (on 401 positions in the $\mathbf{x}_2$ direction). Thus, the sum of these signals leads to the reduction of the noise level, as observed experimentally when temporal signals are averaged to improve the SNR. Indeed, the noisy parts of temporal signals that do not contribute to the synthesis of plane waves are reduced, and the signals that lead to the synthesis of plane waves are amplified. Second, this postprocessing technique filters the contribution of surface acoustic waves, here essentially Rayleigh waves, which propagate at the free surface of medium I in the $\pm\mathbf{x}_2$ direction and do not interact with the bonding. Indeed, the Rayleigh wavelength is equal to 0.59 mm at 5 MHz, and the thickness of medium I is equal to 1.45 mm. This enables analysis of mainly plane waves, which are synthesized from bulk waves reflected from the bonding interface and which contain the necessary information about the mechanical coupling conditions between the two bonded media.

https://doi.org/10.1121/10.0005975

In this section, the results with simulated input data have been presented, and it has been shown that the algorithm illustrated in Fig. 3 allows the identification of interfacial stiffnesses from the amplitudes of the synthesized plane waves. In Sec. V, experimental input data are presented from which the values of K_N and K_T are found.

V. RESOLUTION OF INVERSE PROBLEMS WITH EXPERIMENTAL DATA

The inverse problems were solved in Sec. IV to identify the values of normal and transverse interfacial stiffnesses from simulated signals. In this section, the algorithm presented in Fig. 3 is demonstrated with experimental input data. The aim is to identify two key parameters (K_N and K_T) that model and characterize the practical adhesion between media I and II.

A. Sample preparation

Laser ultrasonic measurements have been performed on three samples. The first specimen was a 1.23-mm-thick aluminum alloy plate of aeronautical quality (6061 grade; Goodfellow, Huntingdon, United Kingdom) of lateral dimensions $150 \times 150\,\text{mm}^2$. Two other samples were composed of 1.45-mm-thick 6061 Al plates bonded with an aeronautical structural adhesive film (AF 191; 3M, Maplewood, MN) on a 20-mm-thick aluminum alloy substrate. The lateral dimensions of these bonded assemblies were similar to those of the first aluminum plate. With regard to the manufacturing process, the aluminum alloy surfaces were first degreased with ethanol. Then, between the 1.45-mm-thick plate and the thicker substrate, strips of material about 5 mm wide were placed on the edges of the surfaces. These strips were used to prevent the glue from leaking during curing and to control the thickness of the epoxy layer (equal to 150 μm). Next, a constant pressure was applied during curing with spring clamps calibrated at 65 N and homogeneously distributed across the sample surface.[7] One bonded sample was manufactured without defects (later called "nominal") and another with an interfacial bonding defect between the top aluminum alloy plate and the epoxy layer. This degradation was introduced by applying one layer of release agent (R.A.; FREKOTE® 44NC™; Henkel Adhesives, Düsseldorf, Germany) with a clean, lint-free cloth on the degreased aluminum alloy surface.[27] This R.A. layer had the effect of degrading the practical adhesion between the aluminum alloy plate and the adhesive. This protocol led to a significant reduction in the structural mechanical strength of the bonding interface while maintaining a mechanical coupling between two parts; they were not detached. These two bonded samples, with and without bonding defects, were cured simultaneously in a laboratory oven at 150 °C for 3 h with ramps up and down (heating and cooling) of 2 °C min^{-1}. The longitudinal static strengths were measured on the order of 20 MPa for the nominal bond and 2 MPa for the sample with adhesion defects. These two bonded assemblies could not be distinguished by acoustic microscopy measurements carried out at 30 MHz.

B. Experimental setup

The laser ultrasonic setup presented in Fig. 5 was used to acquire the experimental B-scans of the three specimens. A Q-switched Nd:YAG laser (SpitLight Compact 400, 532 nm; InnoLas Laser GmbH, Krailling, Germany) delivering 8-ns pulses of 200 mJ with a repetition rate of 10 Hz was used to generate ultrasonic waves in the samples. The laser beam was first attenuated using a $\lambda/2$ plate and a polarizing beamsplitter to adjust the intensity to remain in the thermoelastic (nondestructive) regime. It was then focused onto the surface sample with a cylindrical lens to obtain a line source oriented along the $\mathbf{x}_3$ axis of about 10 mm. The Gaussian profile along the $\mathbf{x}_2$ axis had a FWHM equal to 0.2 mm. To acquire each B-scan, this laser line source was successively displaced to the $2N+1$ positions with the moving stage A shown in Fig. 5. The spatial step δx along the $\mathbf{x}_2$ axis was equal to 0.08 mm. Thus, the line source was moved along 401 positions over a total length of 32 mm. The normal displacement of the surface was measured with a two-wave mixing interferometer (TWM Laser Ultrasound Detector, 1064 nm, bandwidth 0.7–40 MHz; Tecnar, Saint-Bruno-de-Montarville, Quebec, Canada). The laser detection spot, with a diameter at FWHM of 0.6 mm, was always positioned at the center of the generation sources array. Temporal signals were recorded with an HDO4054A oscilloscope (Teledyne LeCroy, Chestnut Ridge, NY) and transferred to a computer for postprocessing. The photodiode, at the output of the Nd:YAG laser cavity, was used to trigger the detection of the interferometer signal by the oscilloscope. For each laser line source position, 500 temporal signals were averaged to increase the SNR $\approx$ 20 dB.

C. Simple case of the free-standing plate

For the aluminum alloy plate of thickness 1.23 mm, the experimental B-scan acquired with this setup is represented in Fig. 6(b). Qualitatively good agreement between the experiment and the simulation performed with the semi-

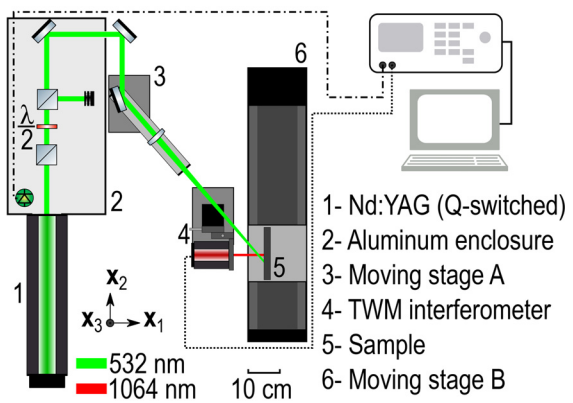

FIG. 5. (Color online) Laser ultrasonic setup for the acquisition of experimental B-scan.

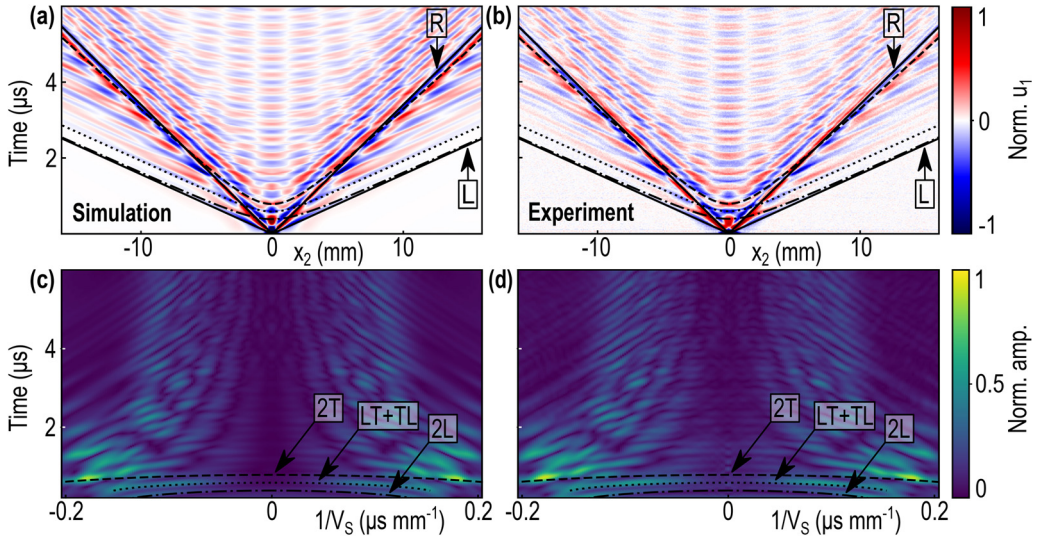

FIG. 6. (Color online) Comparisons between simulation and experiment for the 1.23-mm-thick aluminum alloy plate. (a) Simulated B-scan obtained with the semi-analytic model described in Ref. 48. The normalized (Norm.) normal displacements at the top surface of the aluminum alloy plate are simulated as a function of time and position x_2. (b) Experimental B-scan measured with the setup presented in Fig. 5. The longitudinal wave (L) and the Rayleigh wave (R) are identified with solid lines. (c) and (d) Results of the plane wave synthesis applied on the simulated and experimental B-scans, respectively. The TOF of the reflected synthesized plane waves are identified as dash-dotted line for the 2L longitudinal plane wave, dashed line for the 2T transverse plane wave, and dotted line for the sum of the LT and TL plane waves [previously illustrated in Fig. 1(a)]. amp., amplitude.

analytic model is observed,[48] as shown in Fig. 6(a). The plane wave synthesis was applied on these numerical and experimental B-scans following the same process and parameters as those presented in the previous section. The results are plotted in Figs. 6(c) and 6(d) for the simulation and the experiment, respectively. In these figures, the synthesized plane waves illustrated in Fig. 1(a) can be identified using their TOFs. For instance, four reflected plane waves (2L, LT, TL, 2T) are represented in Figs. 6(c) and 6(d). As time increases, more and more plane waves are synthesized as an incident plane wave is reflected in two waves of longitudinal and transverse polarizations at each interface. This complicates the signal analysis because the total number of synthesized plane waves in medium I is equal to 2^{r+1}, with r being the number of reflections. It is exactly for this reason that the amplitudes of the reflected plane waves were not analyzed separately, but a strategy based on inverse problem solving using all the reflected plane waves was adopted.

Following the same approach as presented in Sec. IV, inverse problems were solved to identify the interfacial stiffnesses (K_N and K_T) of these three samples: the aluminum alloy plate and both bonded assemblies with and without adhesion defects. The experimental B-scans acquired with the laser ultrasonic setup shown in Fig. 5 were used as input data for the algorithm presented in Fig. 3. Next, plane wave synthesis was applied on these temporal signals and compared to the database composed of 1089 semi-analytic simulations with different values of K_N and K_T from 10^{-3} to 10^{5} kN mm^{-3}, with a step of $10^{0.25}$ kN mm^{-3}. These comparisons were based on the MSE to obtain the K_N- and K_T-dependent cost functions plotted in Fig. 7. The red rectangles indicate the minimum of each cost function with an uncertainty margin of ± 0.1 dB, as defined in Sec. IV. This uncertainty margin is used to account for very small local variations of the minimum of the cost function due to noise on temporal B-scans. The extracted values of K_N and K_T are reported in Table II. For the aluminum alloy plate, the values comprised between 10^{-3} and $10^{0.75}$ kN mm^{-3} for K_N, and 10^{-3} and $10^{0.5}$ kN mm^{-3} for K_T. This is consistent with the case presented in Sec. IV where the algorithm was tested

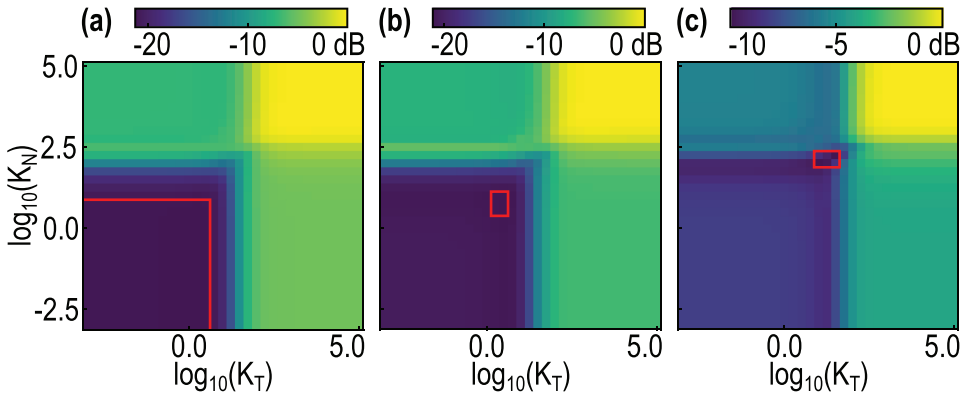

FIG. 7. (Color online) Cost functions obtained when experimental B-scans of (a) an aluminum alloy plate, bonded assemblies Al/epoxy/Al (b) with R.A. and (c) without R.A., are used as input data for the algorithm shown in Fig. 3. The red rectangles indicate the minimum of each cost function with an uncertainty margin of ± 0.1 dB.

https://doi.org/10.1121/10.0005975

TABLE II. The interfacial stiffnesses identified by solving the inverse problem with experimental B-scans as input data in three different experimental cases: aluminum alloy plate, adhesive bonding Al/epoxy/Al with R.A. and without (called nominal bonding).

	Input data		Identified parameters	
Experimental data	K_N	K_T	K_N	K_T
Aluminum alloy plate	—	—	$[10^{-3}, 10^{0.75}]$	$[10^{-3}, 10^{0.5}]$
Bonding with R.A.	—	—	$[10^{0.5}, 10^{1}]$	$[10^{0.25}, 10^{0.5}]$
Nominal bonding	—	—	$[10^{2}, 10^{2.25}]$	$[10^{1}, 10^{1.5}]$

on simulated data with really low values of interfacial stiffnesses $K_N = K_T = 10^{-3}$ kN mm^{-3}. The cost function is represented in Fig. 4(a), and this result is close to what is observed for the experimental case in Fig. 7(a). This first result allows validation of the method on a simple experimental case (free-standing plate) before applying the algorithm on bonded assemblies. It is important to note here that numerous physical phenomena must be accounted for in the simulations, in particular thermal diffusion, to obtain such results with experimental data.

D. Quantification and differentiation of two adhesive bonding conditions: Nominal and degraded

The results are plotted in Fig. 7(b) for the bonded sample with adhesion defects and Fig. 7(c) for the nominal bonding. The extracted values of K_N an K_T are reported in Table II. For the degraded bonding, with the layer of R.A. at one interface, the identified values comprised between $10^{0.5}$ and 10^{1} kN mm^{-3} for K_N and $10^{0.25}$ and $10^{0.5}$ kN mm^{-3} for K_T. For the nominal bonding, the identified values are higher and comprised between 10^{2} and $10^{2.25}$ kN mm^{-3} for K_N and 10^{1} and $10^{1.5}$ kN mm^{-3} for K_T. Therefore, the method enables these two bonded samples to be distinguished, as can be seen from the cost functions in Figs. 7(b) and 7(c).

A covariance analysis was conducted to investigate the sensitivity of K_N and K_T to the cost functions presented in Fig. 7. For fixed values of K_T, the variances and covariances between the cost functions and K_N are plotted in Fig. 8 (on the left). The same was done to study the variances and covariances between the cost functions and K_T for fixed values of K_N (Fig. 8 on the right). For the free-standing aluminum alloy plate and the bonded sample with adhesion defects (R.A.), the variances are higher as a function of K_T for low fixed values of K_N than the variances as a function of K_N for low fixed values of K_T. The cost functions are therefore more sensitive to a change in the K_T than in the K_N parameter. Concerning the nominal bonding, for fixed values of $K_T \in [10^{1}, 10^{1.5}]$ kN mm^{-3} (identified in Table II), the variance of the cost function is lower than the one obtained for fixed values of $K_N \in [10^{2}, 10^{2.25}]$ kN mm^{-3} (identified in Table II). Thus, as in the case of the free-standing aluminum alloy plate and the bonded sample with adhesion defects (R.A.), the cost function is more sensitive to a change in the K_T than in the K_N parameter. The same observations as those exposed previously can be made by

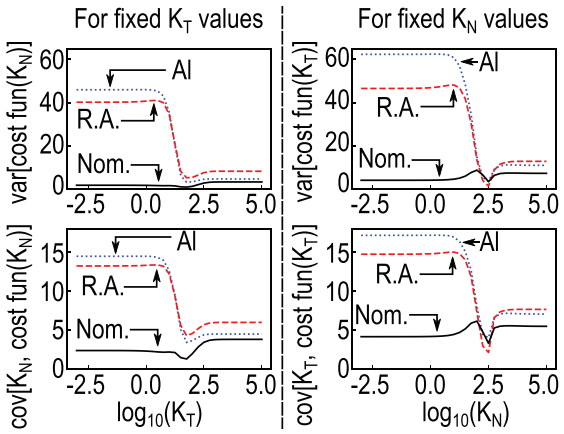

FIG. 8. (Color online) Left: variances (var) and covariances (cov) between the cost functions (presented in Fig. 7) and K_N for fixed values of K_T. Right: var and cov between the cost functions and K_T for fixed values of K_N. Nom., nominal.

looking at the covariances for fixed values of K_T or K_N. The additional information obtained by studying the covariances is that they are always positive. When K_T is fixed, this means that an increase of K_N also tends to an increase of the cost function. When K_N is fixed, an increase of K_T also tends to an increase of the cost function. These observations are consistent with the general shape of the cost functions shown in Fig. 7.

For the bonded sample with adhesion defects, the extracted values of K_N and K_T are close to those achieved for the free-standing aluminum alloy plate. This is due to the fact that the lack of adhesion caused by the layer of R.A. results in weaker mechanical coupling, which has an effect on the amplitudes of the reflected plane waves, making the method sensitive to this type of degradation. Furthermore, in Fig. 7, the minimum of the cost function is higher for the nominal bonding (−10 dB) than for the two other cases (−20 dB). A possible explanation is that the adhesive layer has an influence on the experimental temporal signals that is not fully captured by the simulations of the database. The modeling of the bonding was voluntarily chosen with only two effective parameters related to the mechanical strength of the bonding to avoid the identification of a large set of parameters. In fact, to solve the inverse problem with a finer modeling of the bonding,[26,44] eight parameters must be considered: two interfacial stiffnesses for the upper interface (medium I/adhesive), two others for the lower interface (adhesive/medium II), and four for the adhesive layer [one for the thickness, two for the elastic coefficients (if the adhesive is assumed to be isotropic), and one for the mass density]. To give an order of magnitude considering 30 values for each of the eight parameters, 656.1×10^{9} simulations of laser-generated ultrasound need to be performed to generate the database used for the algorithm presented in Fig. 3 (compared with the 1089 simulations required in this paper). By keeping calculation time within a reasonable range, the model used here and limited to the variation of two key parameters, K_N and K_T, demonstrates the ability to

quantitatively distinguish the three studied specimens from a simplified, although physically justified, model.

VI. CONCLUSION

A laser ultrasonic method has been presented for the NDE of adhesive bonding. Elastic plane waves are synthesized with several propagation angles with respect to the bonding interface. The synthesized plane waves were used to solve an inverse problem to identify normal and transverse interfacial stiffnesses (K_N, K_T) that model the mechanical coupling between two bonded substrates. The developed algorithm was first validated with input data simulated with a semi-analytic model, where Gaussian noise was added. Next, experimental signals acquired on an aluminum alloy plate and on two bonded assemblies (with and without adhesion defects) were used as input data. This method allowed for distinguishing these three specimens by finding the minima of cost functions on the basis of the differences between the input data and a database composed of semi-analytic simulations for a large set of K_N and K_T.

Concerning the limits of this approach, the mechanical properties of the bonded substrates must be known to obtain accurate simulations of the ultrasound propagation necessary for the creation of the database. Furthermore, this method provides average values of K_N and K_T for the scanned area (32 mm in our experiments); no local bonding defects can be detected. In addition, the top plate, where the laser generation and detection are performed, must be free of imperfections as is assumed in the model. However, such imperfections can be easily detected since the detection of elastic waves with shorter TOFs than those reflected from the bonding interface would be a sign of such imperfections.

In terms of prospects, other methods of comparison between the input data and the database could be tested, such as structural similarity index measure (SSIM)[59,60] or others. Moreover, the presented method could be implemented with an even more complete semi-analytic model taking the thickness, the elastic coefficients, and the mass density of the adhesive into account. The introduction of new parameters will greatly complicate the resolution of the inverse problem by considerably increasing the number of simulations required to create the database (see Sec. V). A thoughtful analysis of how the parameter dependence/independence affects the solution of the inverse problem could eventually permit a decrease in the number of degrees of freedom in the minimization process. Succeeding in doing so would allow consideration of reflected plane waves of higher frequencies (above 5 MHz) and, therefore, would ensure that a more accurate description of the bonded assembly be obtained.

[1]C. C. H. Guyott, P. Cawley, and R. D. Adams, "The non-destructive testing of adhesively bonded structure: A review," J. Adhes. **20**(2), 129–159 (1986).
[2]R. D. Adams and B. W. Drinkwater, "Nondestructive testing of adhesively-bonded joints," NDT&E Int. **30**(2), 93–98 (1997).
[3]M. D. Bode, M. J. Holle, and D. Westlund (2015). "Literature review of weak adhesive bond fabrication and nondestructive inspection for strength measurement." http://www.tc.faa.gov/its/worldpac/techrpt/tc14-39.pdf (Last viewed 23 August 2021)
[4]C. Meola and G. M. Carlomagno, "Application of infrared thermography to adhesion science," J. Adhes. Sci. Technol. **20**(7), 589–632 (2006)
[5]R. C. Tighe, J. M. Dulieu-Barton, and S. Quinn, "Identification of kissing defects in adhesive bonds using infrared thermography," Int. J. Adhes. Adhes. **64**, 168–178 (2016)
[6]L. Berthe, M. Arrigoni, M. Boustie, J. P. Cuq-Lelandais, C. Broussillou, G. Fabre, M. Jeandin, V. Guipont, and M. Nivard, "State-of-the-art laser adhesion test (LASAT)," Nondestruct. Test. Eva. **26**(3-4), 303–317 (2011)
[7]M. Ducousso, S. Bardy, Y. Rouchausse, T. Bergara, F. Jenson, L. Berthe, L. Videau, and N. Cuvillier, "Quantitative evaluation of the mechanical strength of titanium/composite bonding using laser-generated shock waves," Appl. Phys. Lett. **112**(11), 111904 (2018).
[8]H. G. Tattersall, "The ultrasonic pulse-echo technique as applied to adhesion testing," J. Phys. D Appl. Phys. **6**(7), 819–832 (1973).
[9]S. I. Rokhlin and D. Marom, "Study of adhesive bonds using low-frequency obliquely incident ultrasonic waves," J. Acoust. Soc. Am. **80**(2), 585–590 (1986).
[10]A. Pilarski and J. L. Rose, "A transverse-wave ultrasonic oblique-incidence technique for interfacial weakness detection in adhesive bonds," J. Appl. Phys. **63**(2), 300–307 (1988).
[11]P. B. Nagy, "Ultrasonic detection of kissing bonds at adhesive interfaces," J. Adhes. Sci. Technol. **5**(8), 619–630 (1991).
[12]E. Siryabe, M. Rénier, A. Meziane, J. Galy, and M. Castaings, "Apparent anisotropy of adhesive bonds with weak adhesion and non-destructive evaluation of interfacial properties," Ultrasonics **79**, 34–51 (2017).
[13]W.-L. Wu, X.-G. Wang, Z.-C. Huang, and N.-X. Wu, "Measurements of the weak bonding interfacial stiffness by using air-coupled ultrasound," AIP Adv. **7**(12), 125316 (2017).
[14]M. Schoenberg, "Elastic wave behavior across linear slip interfaces," J. Acoust. Soc. Am. **68**(5), 1516–1521 (1980).
[15]J.-M. Baik and R. B. Thompson, "Ultrasonic scattering from imperfect interfaces: A quasi-static model," J. Nondestr. Eval. **4**(3-4), 177–196 (1984).
[16]S. I. Rokhlin and Y. J. Wang, "Analysis of boundary conditions for elastic wave interaction with an interface between two solids," J. Acoust. Soc. Am. **89**(2), 503–515 (1991).
[17]N. Mori, N. Matsuda, and T. Kusaka, "Effect of interfacial adhesion on the ultrasonic interaction with adhesive joints: A theoretical study using spring-type interfaces," J. Acoust. Soc. Am. **145**(6), 3541–3550 (2019).
[18]A. I. Lavrentyev and S. I. Rokhlin, "Determination of elastic moduli, density, attenuation, and thickness of a layer using ultrasonic spectroscopy at two angles," J. Acoust. Soc. Am. **102**(6), 3467–3477 (1997).
[19]L. Wang, B. Xie, and S. I. Rokhlin, "Determination of embedded layer properties using adaptive time-frequency domain analysis," J. Acoust. Soc. Am. **111**(6), 2644–2653 (2002).
[20]A. Baltazar, L. Wang, B. Xie, and S. I. Rokhlin, "Inverse ultrasonic determination of imperfect interfaces and bulk properties of a layer between two solids," J. Acoust. Soc. Am. **114**(3), 1424–1434 (2003).
[21]B. L. Crom and M. Castaings, "Shear horizontal guided wave modes to infer the shear stiffness of adhesive bond layers," J. Acoust. Soc. Am. **127**(4), 2220–2230 (2010).
[22]M. Castaings, "SH ultrasonic guided waves for the evaluation of interfacial adhesion," Ultrasonics **54**(7), 1760–1775 (2014).
[23]R. Seifried, L. J. Jacobs, and J. Qu, "Propagation of guided waves in adhesive bonded components," NDT&E Int. **35**(5), 317–328 (2002).
[24]C. Gauthier, M. Ech-Cherif El-Kettani, J. Galy, M. Predoi, and D. Leduc, "Structural adhesive bonding characterization using guided Lamb waves and the vertical modes," Int. J. Adhes. Adhes. **98**, 102467 (2020).
[25]C. Prada, O. Balogun, and T. Murray, "Laser-based ultrasonic generation and detection of zero-group velocity Lamb waves in thin plates," Appl. Phys. Lett. **87**, 194109 (2005).
[26]S. Mezil, F. Bruno, S. Raetz, J. Laurent, D. Royer, and C. Prada, "Investigation of interfacial stiffnesses of a tri-layer using zero-group velocity Lamb modes," J. Acoust. Soc. Am. **138**(5), 3202–3209 (2015).
[27]R. Hodé, S. Raetz, J. Blondeau, N. Chigarev, N. Cuvillier, V. Tournat, and M. Ducousso, "Nondestructive evaluation of structural adhesive bonding using the attenuation of zero-group-velocity Lamb modes," Appl. Phys. Lett. **116**(10), 104101 (2020).

[28]J. Spytek, A. Ziaja-Sujdak, K. Dziedziech, L. Pieczonka, I. Pelivanov, and L. Ambrozinski, "Evaluation of disbonds at various interfaces of adhesively bonded aluminum plates using all-optical excitation and detection of zero-group velocity Lamb waves," NDT&E Int. **112**, 102249 (2020).
[29]F. Reverdy and B. Audoin, "Elastic constants determination of anisotropic materials from phase velocities of acoustic waves generated and detected by lasers," J. Acoust. Soc. Am. **109**(5), 1965–1972 (2001).
[30]F. Reverdy and B. Audoin, "Ultrasonic measurement of elastic constants of anisotropic materials with laser source and laser receiver focused on the same interface," J. Appl. Phys. **90**(9), 4829–4835 (2001).
[31]Y. H. Berthelot and I. J. Busch-Vishniac, "Thermoacoustic radiation of sound by a moving laser source," J. Acoust. Soc. Am. **81**(2), 317–327 (1987).
[32]R. Ing, M. Fink, and F. Gires, "Directivity patterns of a moving thermoelastic source in solid media," IEEE T. Ultrason. Ferr. **39**(2), 285–292 (1992).
[33]B. W. Drinkwater and P. D. Wilcox, "Ultrasonic arrays for non-destructive evaluation: A review," NDT&E Int. **39**(7), 525–541 (2006).
[34]J. S. Steckenrider, T. W. Murray, J. W. Wagner, and J. B. Deaton, "Sensitivity enhancement in laser ultrasonics using a versatile laser array system," J. Acoust. Soc. Am. **97**(1), 273–279 (1995).
[35]J. U. White, "Long optical paths of large aperture," J. Opt. Soc. Am. **32**, 285–288 (1942).
[36]J. Vogel, A. Bruinsma, and A. Berkhout, *Beamsteering of Laser-Generated Ultrasound* (Elsevier, Amsterdam, 1987), pp. 141–152.
[37]J. Jarzynski and Y. H. Berthelot, "The use of optical fibers to enhance the laser generation of ultrasonic waves," J. Acoust. Soc. Am. **85**(1), 158–162 (1989).
[38]C. Pei, D. Yi, T. Liu, X. Kou, and Z. Chen, "Fully noncontact measurement of inner cracks in thick specimen with fiber-phased-array laser ultrasonic technique," NDT&E Int. **113**, 102273 (2020).
[39]M.-H. Noroy, D. Royer, and M. Fink, "The laser-generated ultrasonic phased array: Analysis and experiments," J. Acoust. Soc. Am. **94**(4), 1934–1943 (1993).
[40]M.-H. Noroy, D. Royer, and M. Fink, "Transient elastic wave generation by an array of thermoelastic sources," Appl. Phys. Lett. **63**(24), 3276–3278 (1993).
[41]M.-H. Noroy, D. Royer, and M. Fink, "Shear-wave focusing with a laser-ultrasound phased-array," IEEE T. Ultrason. Ferr. **42**(6), 981–988 (1995).
[42]T. Murray, J. Deaton, and J. Wagner, "Experimental evaluation of enhanced generation of ultrasonic waves using an array of laser sources," Ultrasonics **34**(1), 69–77 (1996).
[43]J. P. Jones and J. S. Whittier, "Waves at a flexibly bonded interface," J. Appl. Mech. **34**(4), 905–909 (1967).
[44]V. Vlasie and M. Rousseau, "Acoustical validation of the rheological models for a structural bond," Wave Motion **37**(4), 333–349 (2003).
[45]W. T. Thomson, "Transmission of elastic waves through a stratified solid medium," J. Appl. Phys. **21**(2), 89–93 (1950).
[46]L. M. Brekhovskikh, *Waves in Layered Media*, 2nd ed. (Academic Press, Cambridge, MA, 1980).
[47]A. Cheng, T. W. Murray, and J. D. Achenbach, "Simulation of laser-generated ultrasonic waves in layered plates," J. Acoust. Soc. Am. **110**(2), 848–855 (2001).
[48]R. Hodé, M. Ducousso, N. Cuvillier, V. Gusev, V. Tournat, and S. Raetz, "Laser ultrasonics in a multilayer structure: Semi-analytic model and simulated examples," J. Acoust. Soc. Am. **150**, 2065–2075 (2021).
[49]T. Stratoudaki, M. Clark, and P. D. Wilcox, "Laser induced ultrasonic phased array using full matrix capture data acquisition and total focusing method," Opt. Express **24**(19), 21921–21938 (2016).
[50]A. Viel and B. Audoin, "Directivity of GHz shear acoustic waves launched by the absorption of short laser pulses at the interface between a transparent and an absorbing material," J. Appl. Phys. **123**(4), 043102 (2018).
[51]S. Raetz, T. Dehoux, M. Perton, and B. Audoin, "Acoustic beam steering by light refraction: Illustration with directivity patterns of a tilted volume photoacoustic source," J. Acoust. Soc. Am. **134**(6), 4381–4392 (2013).
[52]B. Audoin and S. Guilbaud, "Acoustic waves generated by a line source in a viscoelastic anisotropic medium," Appl. Phys. Lett. **72**(7), 774–776 (1998).
[53]B. Audoin, H. Meri, and C. Rossignol, "Two-dimensional diffraction of plasma, thermal, and elastic waves generated by an infrared laser pulse in semiconductors," Phys. Rev. B **74**(21), 214304 (2006).
[54]Z. Shen, B. Xu, X. Ni, and J. Lu, "Numerical simulation of laser-generated ultrasonic waves in layered plates," J. Phys. D: Appl. Phys. **37**(17), 2364–2370 (2004).
[55]G. Yan, S. Raetz, N. Chigarev, J. Blondeau, V. E. Gusev, and V. Tournat, "Cumulative fatigue damage in thin aluminum films evaluated non-destructively with lasers via zero-group-velocity Lamb modes," NDT&E Int. **116**, 102323 (2020).
[56]I. A. Veres, T. Berer, and P. Burgholzer, "Numerical modeling of thermoelastic generation of ultrasound by laser irradiation in the coupled thermoelasticity," Ultrasonics **53**(1), 141–149 (2013).
[57]See supplementary material at https://www.scitation.org/doi/suppl/10.1121/10.0005975 for the simplification of the transfer matrix for a layer with homogeneous, linear, and isotropic mechanical properties and videos of the results of the semi-analytic simulations.
[58]C. B. Scruby, R. J. Dewhurst, D. A. Hutchins, and S. B. Palmer, "Quantitative studies of thermally generated elastic waves in laser-irradiated metals," J. Appl. Phys. **51**(12), 6210–6216 (1980).
[59]Z. Wang, A. Bovik, H. Sheikh, and E. Simoncelli, "Image quality assessment: From error visibility to structural similarity," IEEE T. Image Process. **13**(4), 600–612 (2004).
[60]M. Ducousso, A. Dalodière, and A. Baillard, "Evaluation of the thermal aging of aeronautical composite materials using Lamb waves," Ultrasonics **94**, 174–182 (2019).